Data formation process and image reconstruction methods for the Spectrometer/Telescope for Imaging X-rays on-board Solar Orbiter

Università di Genova
DIMA | Dipartimento di Matematica

Anna Volpara, Paolo Massa, Emma Perracchione, Federico Benvenuto, Andrea Francesco Battaglia, Säm Krucker, Gordon Hurford, Michele Piana, Anna Maria Massone

Workshop "Science with current and future solar physics missions"
February 2, 2023

Outline

1. STIX data formation process
2. Image reconstruction methods
3. Results

STIX - Spectrometer/Telescope for Imaging X-rays

STIX: Spectrometer/Telescope for Imaging X-rays

Goal: provide information on electrons accelerated during a solar flare and on the plasma temperature

Data: complex values of specific Fourier components of the flaring X-ray source.

STIX - Spectrometer/Telescope for Imaging X-rays

STIX: Spectrometer/Telescope for Imaging X-rays

Goal: provide information on electrons accelerated during a solar flare and on the plasma temperature

Data: complex values of specific Fourier components of the flaring X-ray source.

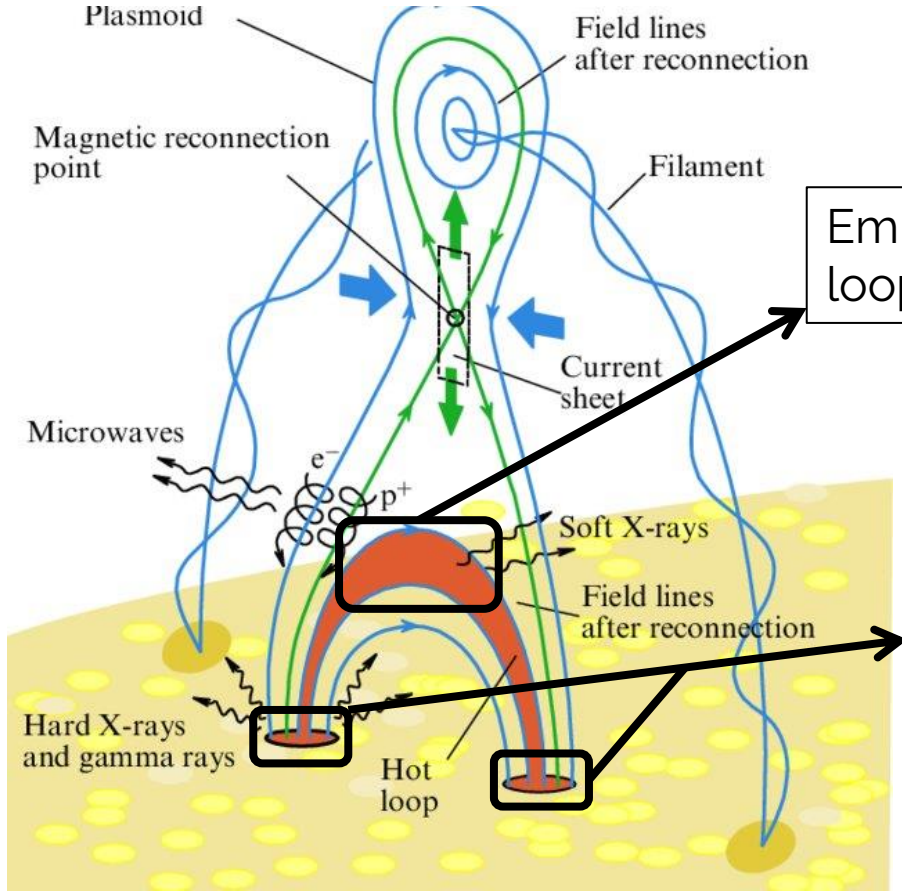

Emission of soft X-rays from loop top due to heating

Emission of hard X-rays from footpoints due to bremsstrahlung mechanisms

Holman (2012)

STIX - Spectrometer/Telescope for Imaging X-rays

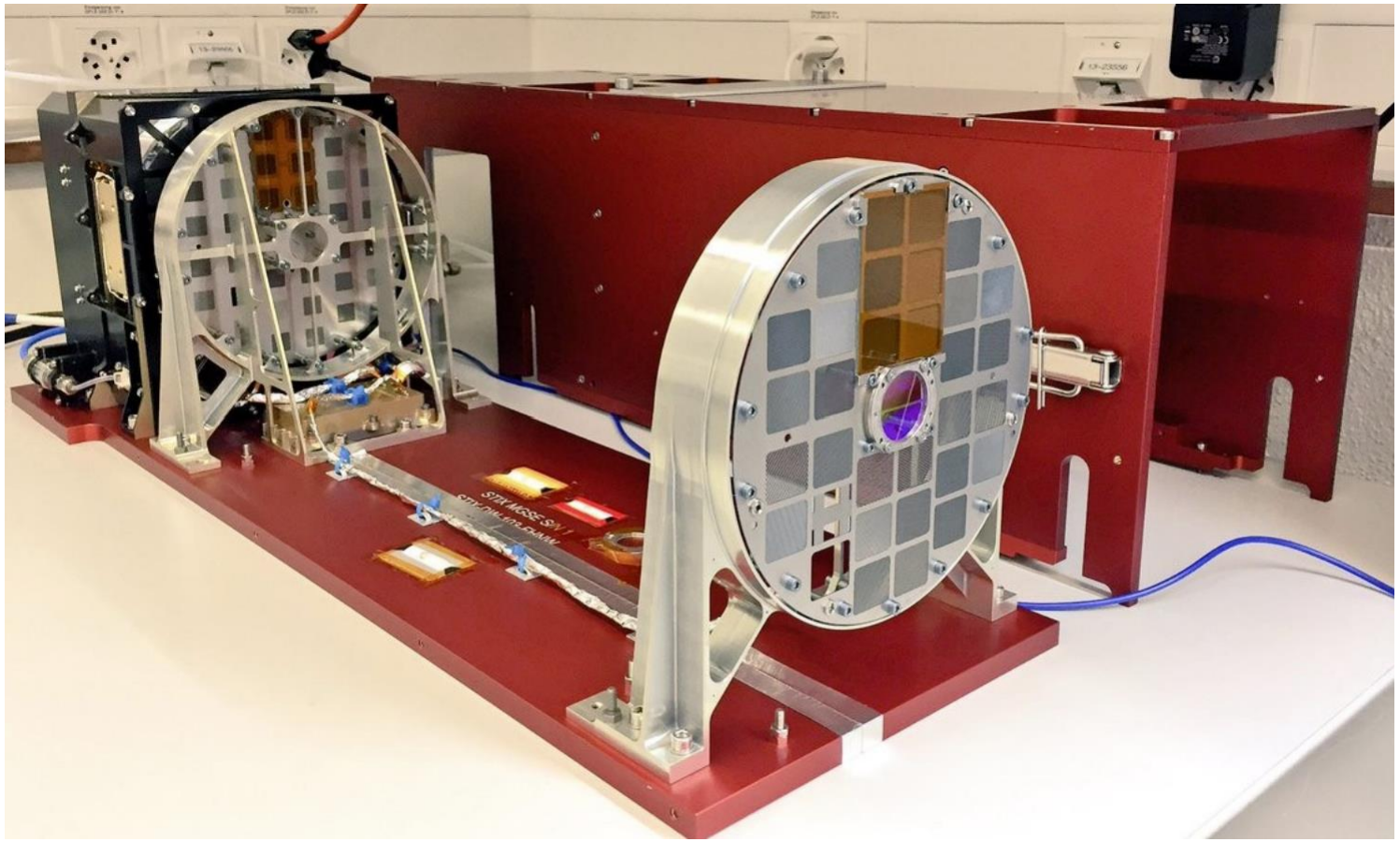

Figure: STIX before being assembled on Solar Orbiter
(Krucker et al., 2020).

STIX - Spectrometer/Telescope for Imaging X-rays

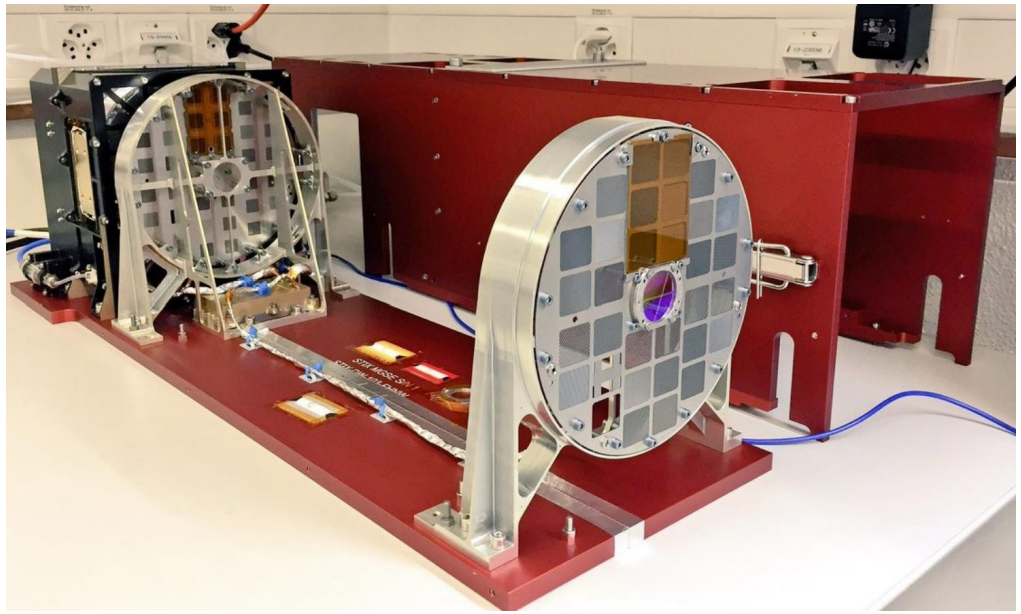

Figure: STIX before being assembled on Solar Orbiter (Krucker et al., 2020).

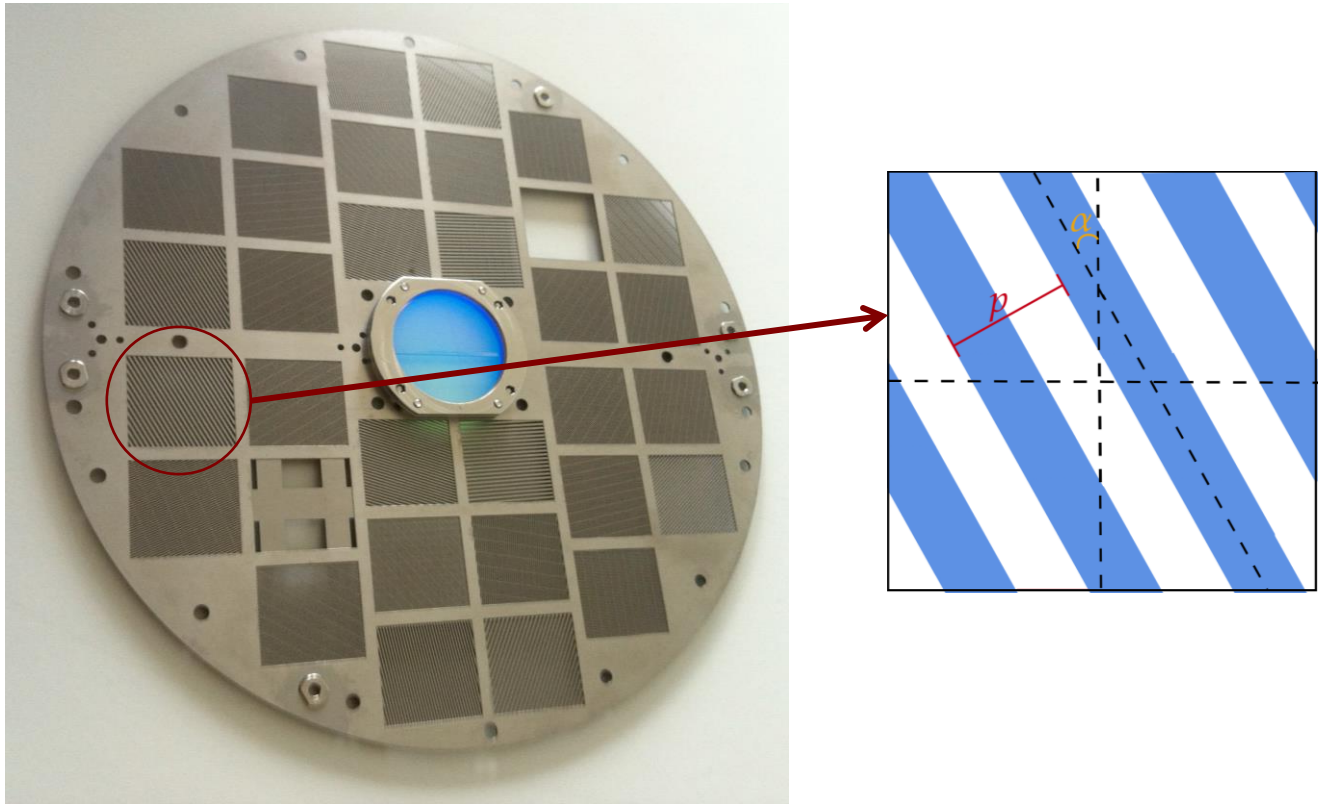

Figure: front and the rear grids before being assembled on the spacecraft (*left panel*), schematic of a grid window (*right panel*).

STIX - Spectrometer/Telescope for Imaging X-rays

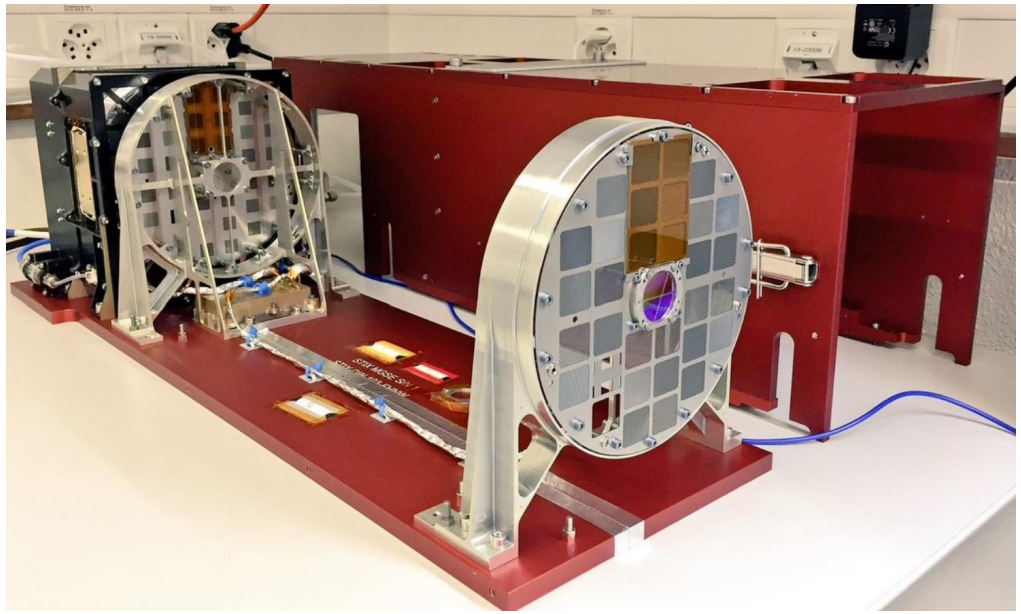

Figure: STIX before being assembled on Solar Orbiter (Krucker et al., 2020).

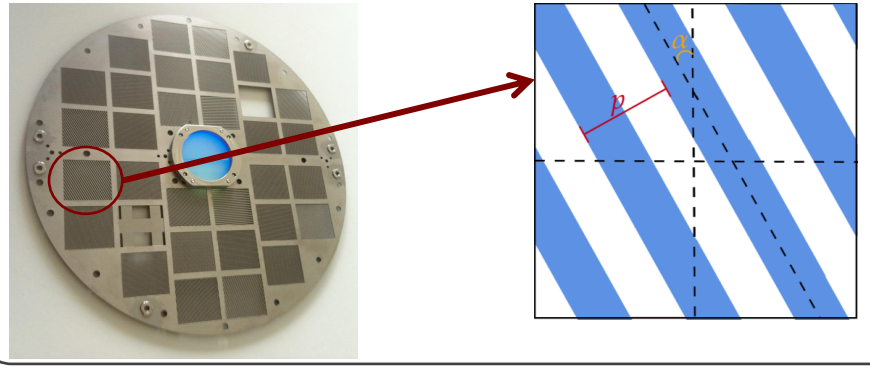

Figure: front and the rear grids before being assembled on the spacecraft (*left panel*), schematic of a grid window (*right panel*).

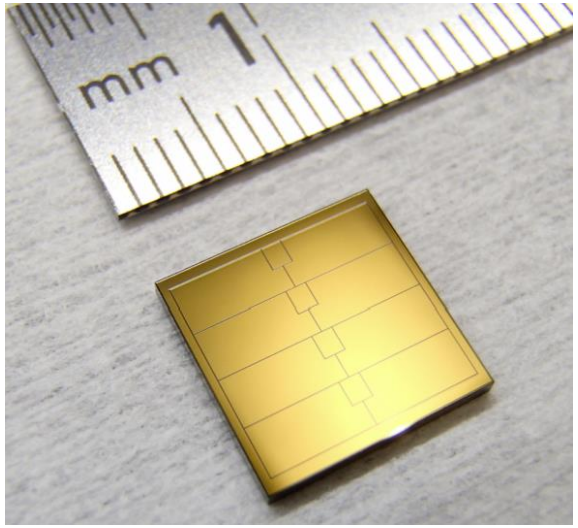

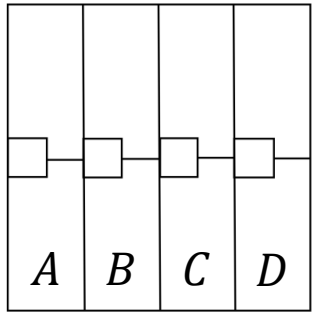

Figure: STIX detector (*left panel*) schematic of a detector (*right panel*).

STIX - Spectrometer/Telescope for Imaging X-rays

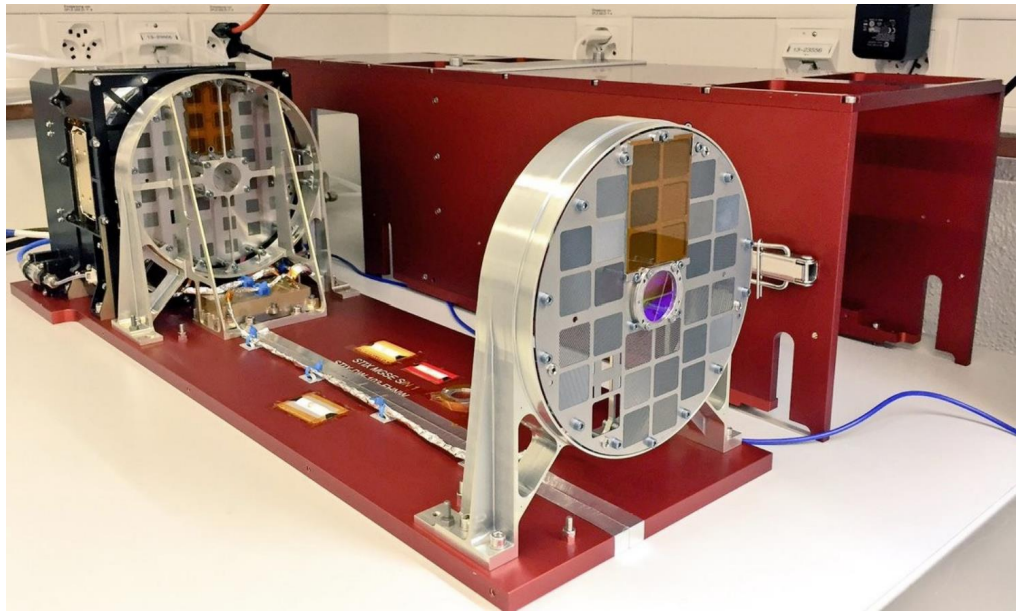

Figure: STIX before being assembled on Solar Orbiter (Krucker et al., 2020).

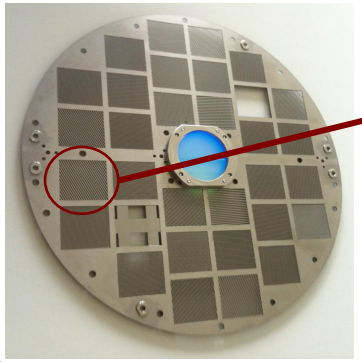

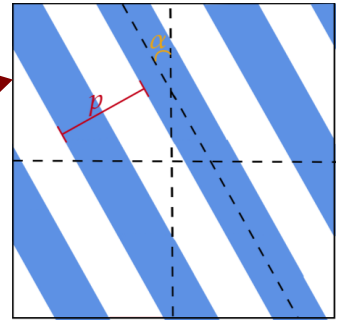

Figure: front and the rear grids before being assembled on the spacecraft (*left panel*), schematic of a grid window (*right panel*).

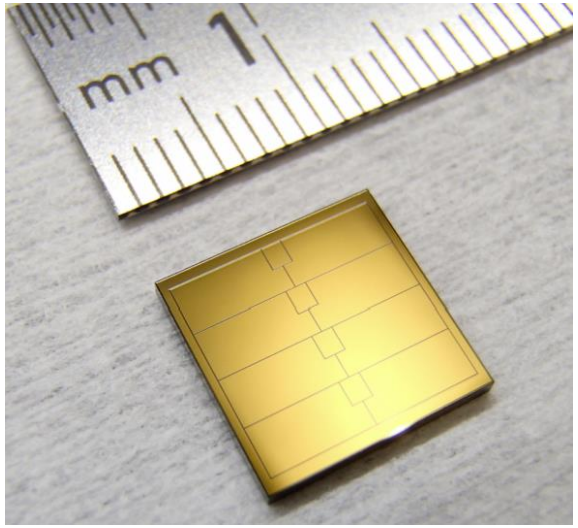

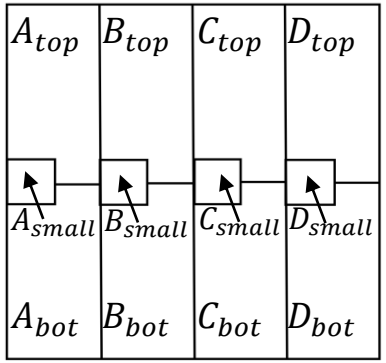

Figure: STIX detector (*left panel*) schematic of a detector (*right panel*).

STIX - Spectrometer/Telescope for Imaging X-rays

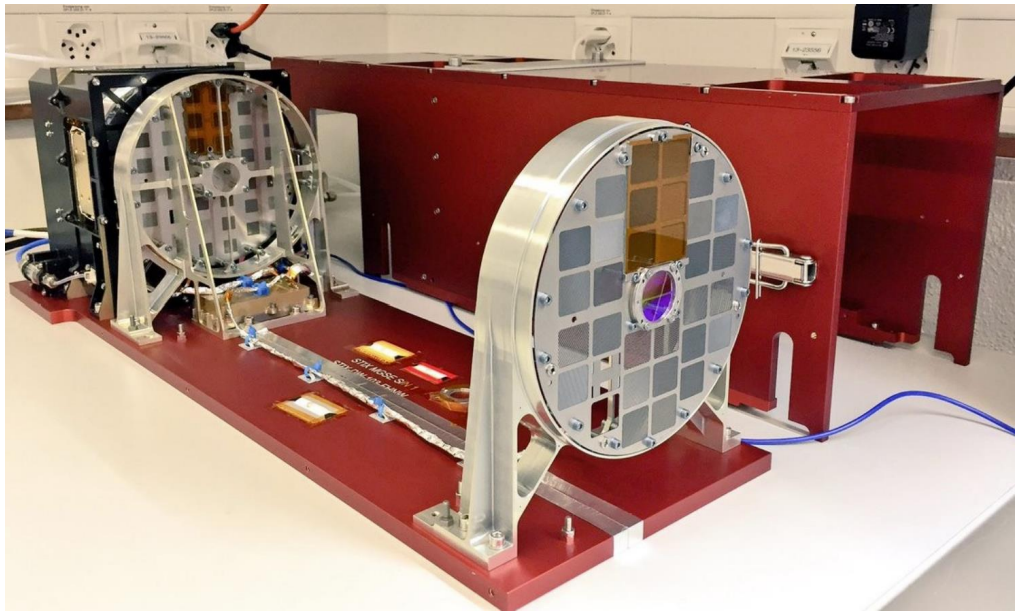

Figure: STIX before being assembled on Solar Orbiter (Krucker et al., 2020).

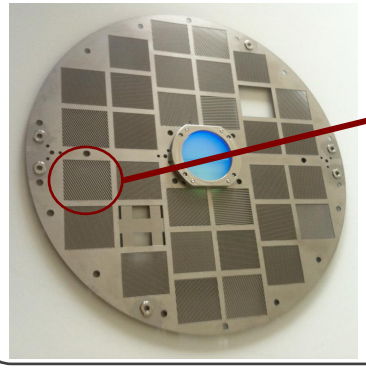

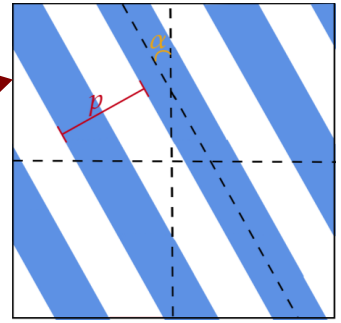

Figure: front and the rear grids before being assembled on the spacecraft (*left panel*), schematic of a grid window (*right panel*).

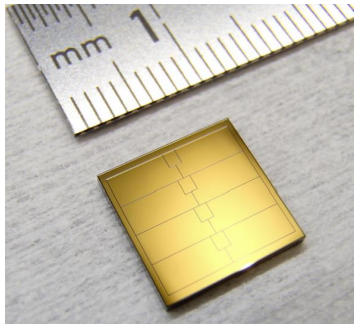

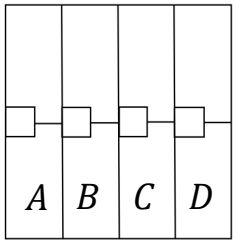

Figure: STIX detector (*left panel*) schematic of a detector (*right panel*).

Front grid + *Rear grid* + *detector* } Sub-collimator

STIX data formation process

Front and rear grid of the same sub-collimator have slightly different pitch and orientation.

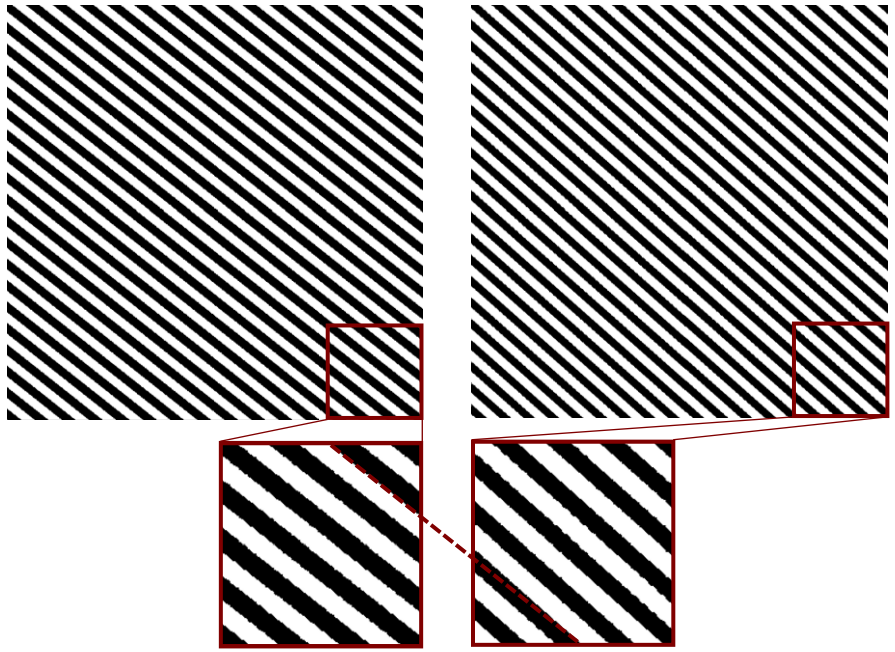

Figure: simulation of the flux transmitted through the front (*left panels*) and rear (*right panels*) windows.

The transmitted X-ray photon flux creates a **Moiré pattern**.

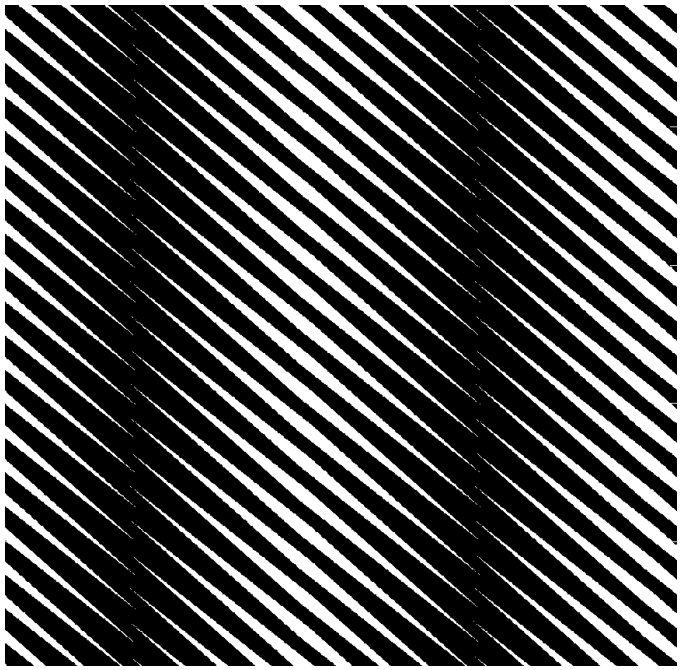

Figure: Moiré pattern created by the superimposition of the flux transmitted through the windows.

Moiré pattern

The amplitude of a Moiré pattern is sensitive to the source size

X-ray source

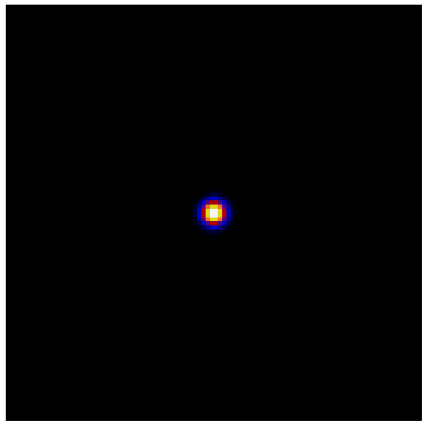

FWHM from 12 to 120 arcsec

Resolution: 178.6 arcsec

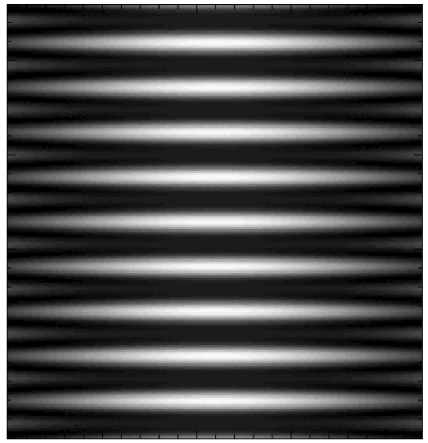

Resolution: 61.0 arcsec

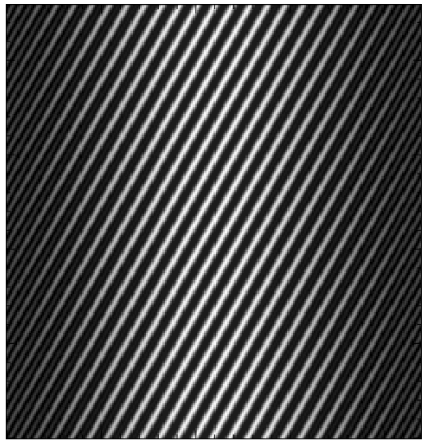

Resolution: 20.9 arcsec

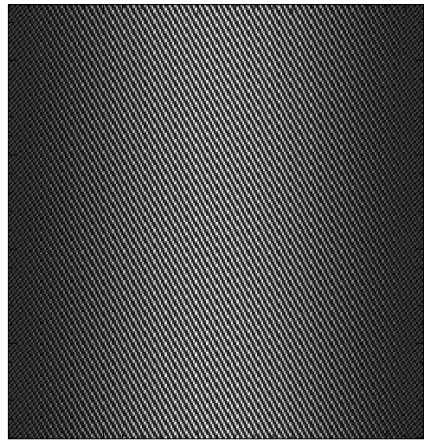

Courtesy P. Massa

Moiré pattern

The phase of a Moiré pattern is sensitive to the source location

X-ray source

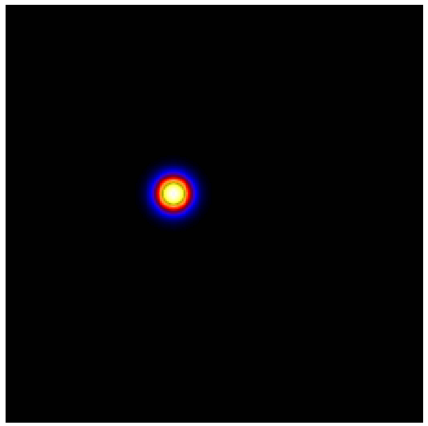

Resolution: 178.6 arcsec

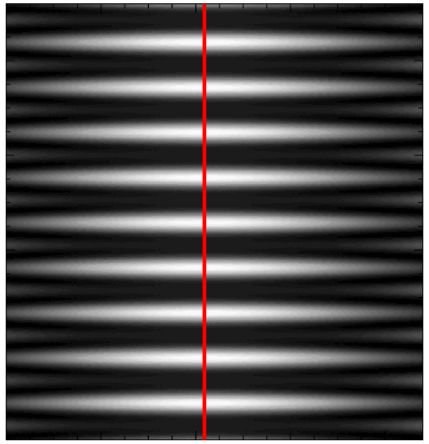

Resolution: 61.0 arcsec

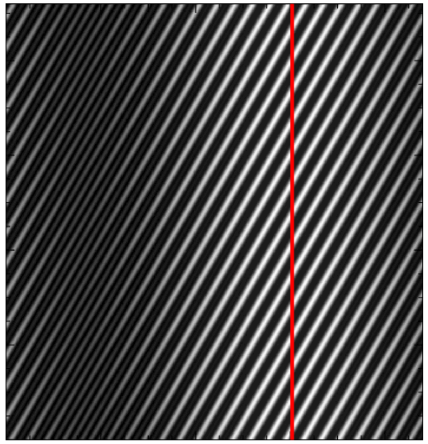

Resolution: 20.9 arcsec

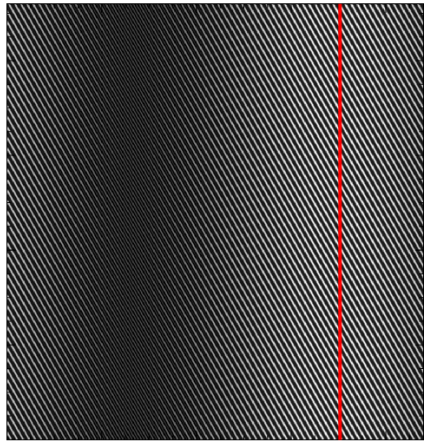

Courtesy P. Massa

STIX data formation process

Image reconstruction problem for STIX:

$$\mathcal{F}\phi = \mathsf{V} \tag{1}$$

STIX data formation process

Image reconstruction problem for STIX:

$$\mathcal{F}\phi = \mathrm{V} \qquad (1)$$

Intensity of the X-ray photon flux emitted from (x, y) on the Sun

STIX data formation process

Image reconstruction problem for STIX:

$$\mathcal{F}\phi = \mathrm{V} \qquad (1)$$

Array containing the N_V complex values of the visibilities measured by STIX

$$|V| \propto \sqrt{(C-A)^2 + (D-B)^2}$$

$$\psi = \mathrm{atan}\left(\frac{D-B}{C-A}\right) + 45° + \psi_{\mathrm{calib}}$$

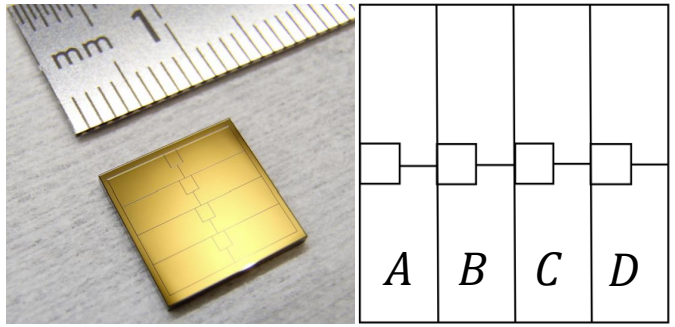

Figure: STIX detector (*left panel*) schematic of a detector (*right panel*).

STIX data formation process

Image reconstruction problem for STIX:

$$\mathcal{F}\phi = \mathsf{V} \qquad (1)$$

The Fourier Transform defined by:

$$(\mathcal{F}\phi)_k = \iint \phi(x,y)\exp\left(2\pi i(xu_k + yv_k)\right)\,dx\,dy \quad k = 1,\ldots,N_v$$

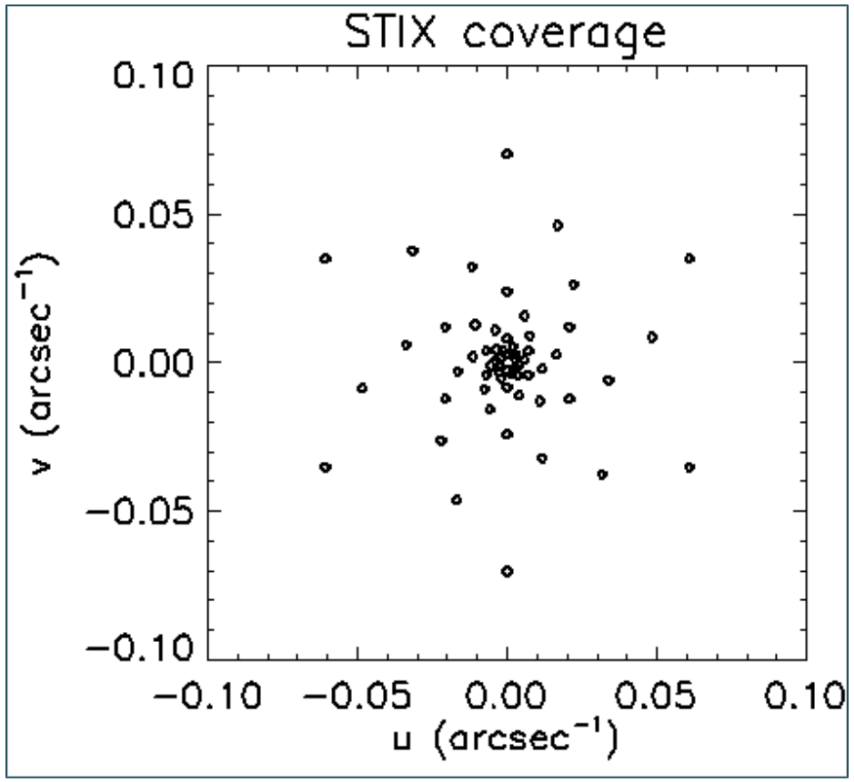

Results – August 26, 2021

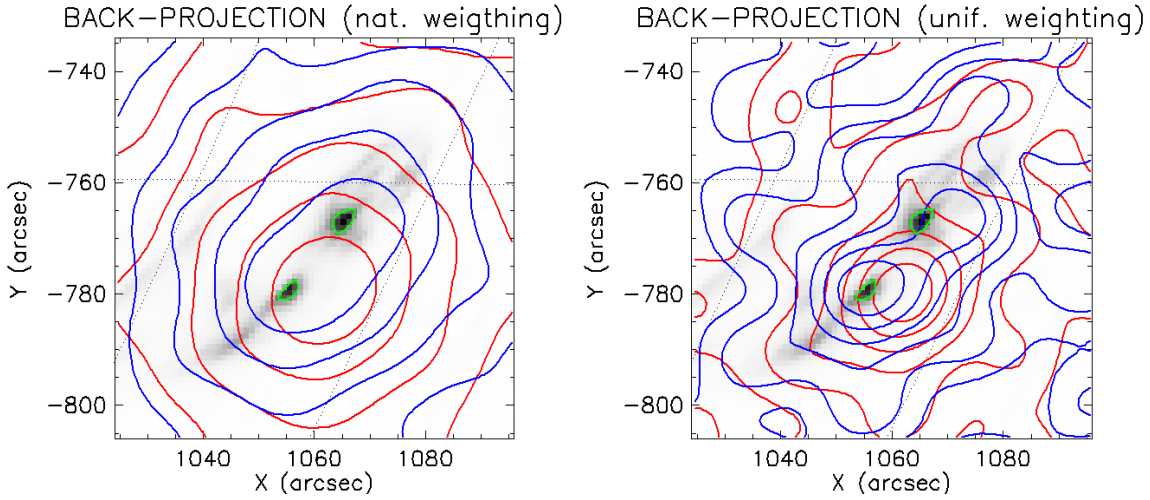

- Active region: AR2680
- 23:19:00 UT: GOES C4.0

STIX 6 – 10 keV
STIX 15 – 25 keV
AIA 1600 Å rotated

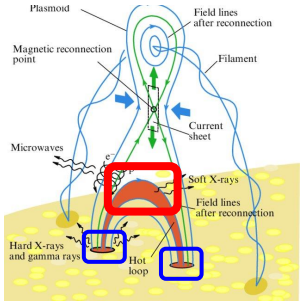

Figure: reconstructions provided by Back-projection overlaid on the rotated AIA maps of the same events. Contour levels of the reconstructed thermal and non-thermal X-ray emissions are plotted in red and blue, respectively.

Results – August 26, 2021

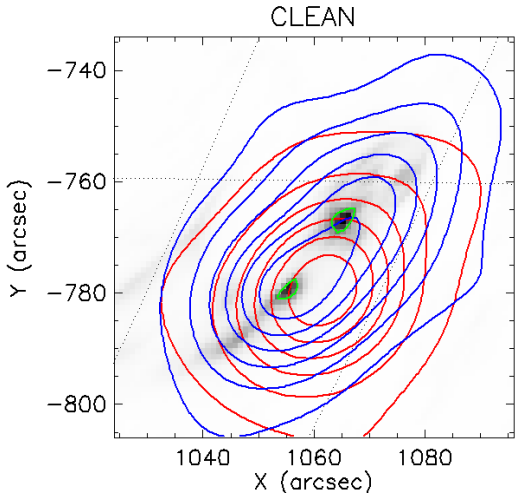

- Active region: AR2680
- 23:19:00 UT: GOES C4.0

STIX 6 – 10 keV
STIX 15 – 25 keV
AIA 1600 Å rotated

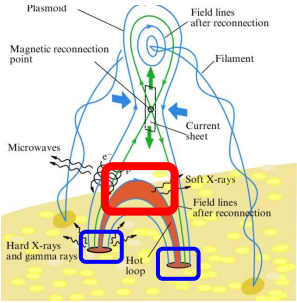

Figure: reconstructions provided by CLEAN overlaid on the rotated AIA maps of the same events. Contour levels of the reconstructed thermal and non-thermal X-ray emissions are plotted in red and blue, respectively.

CLEAN (Högbom, Astronomy and Astrophysics Supplement, 1974)

Deconvolution algorithm:

- Creates two maps:
  - DIRTY MAP (back-projection)
  - CLEAN COMPONENT (zero map)

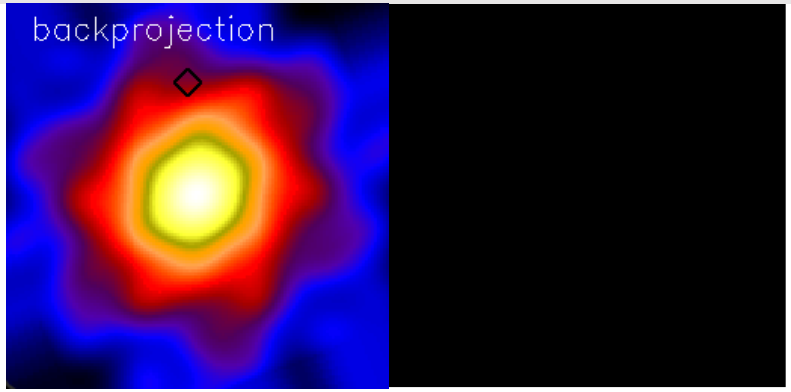

CLEAN (Högbom, Astronomy and Astrophysics Supplement, 1974)

Deconvolution algorithm:

- Creates two maps:
  - DIRTY MAP (back-projection)
  - CLEAN COMPONENT (zero map)

- Finds maximum of the dirty map and add clean component in the clean component map.
- Subtracts a fraction of the PSF from the dirty map.

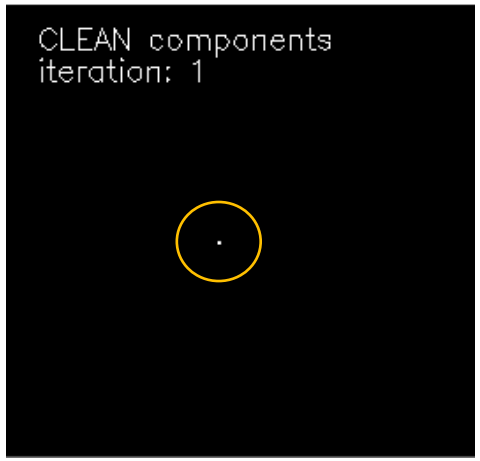

CLEAN (Högbom, Astronomy and Astrophysics Supplement, 1974)

Deconvolution algorithm:

- Creates two maps: DIRTY MAP (back-projection), CLEAN COMPONENT (zero map)
- Finds maximum of the dirty map and add clean component in the clean component map.
- Subtracts a fraction of the PSF from the dirty map.
- Iterates

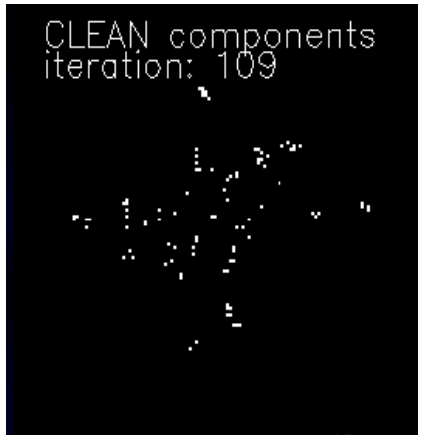

Convolution with clean beam

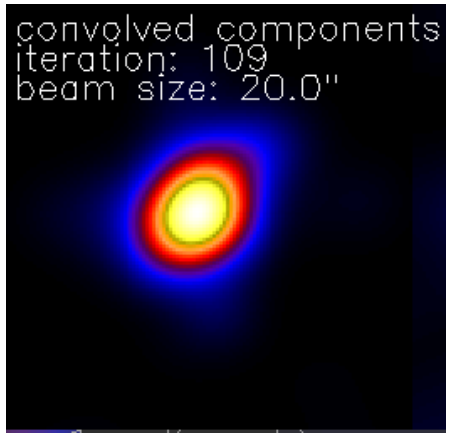

Adds residuals

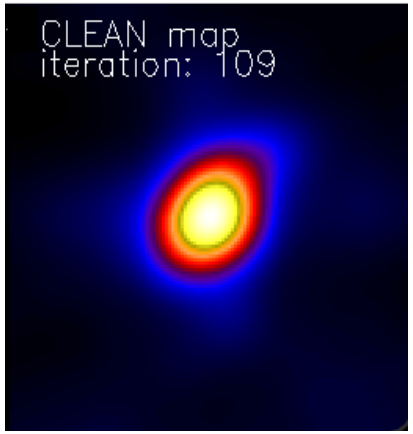

Results – August 26, 2021

- Active region: AR2680
- 23:19:00 UT: GOES C4.0

STIX 6 – 10 keV
STIX 15 – 25 keV
AIA 1600 Å rotated

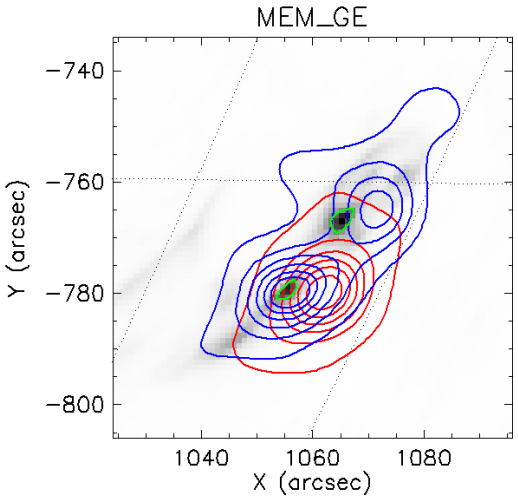

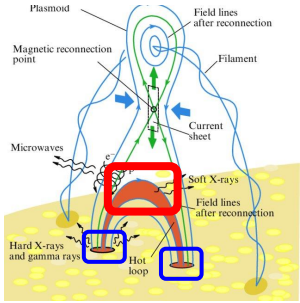

Figure: reconstructions provided by MEM_GE overlaid on the rotated AIA maps of the same events. Contour levels of the reconstructed thermal and non-thermal X-ray emissions are plotted in red and blue, respectively.

MEM_GE (Massa et al., The Astrophysical Journal, 2020)

Solves:

$$\underset{\phi}{\text{argmin}} \quad \chi^2(\phi) - \lambda H(\phi)$$

with $\phi \succeq 0$

F=0

$$\chi^2(\phi) = \sum_i \frac{|(\mathcal{F}\phi)_i - V_i|^2}{\sigma_i^2}$$

$$H(\phi) = -\sum_j \phi_j \log\left(\frac{\phi_j}{me}\right)$$

$$F = \sum_j \phi_j - F'$$

Results – August 26, 2021

- Active region: AR2680
- 23:19:00 UT: GOES C4.0

STIX 6 – 10 keV
STIX 15 – 25 keV
AIA 1600 Å rotated

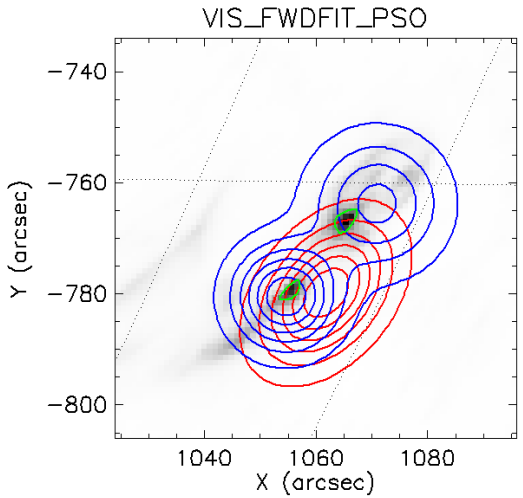

Figure: reconstructions provided by VIS_FWDFIT_PSO overlaid on the rotated AIA maps of the same events. Contour levels of the reconstructed thermal and non-thermal X-ray emissions are plotted in red and blue, respectively.

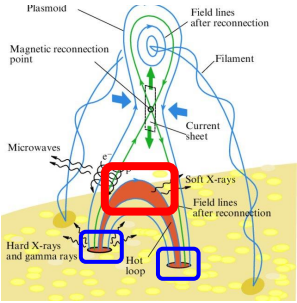

VIS_FWDFIT_PSO (Volpara et al., Astronomy and Astrophysics, 2022)

Choose a parametric shape among:

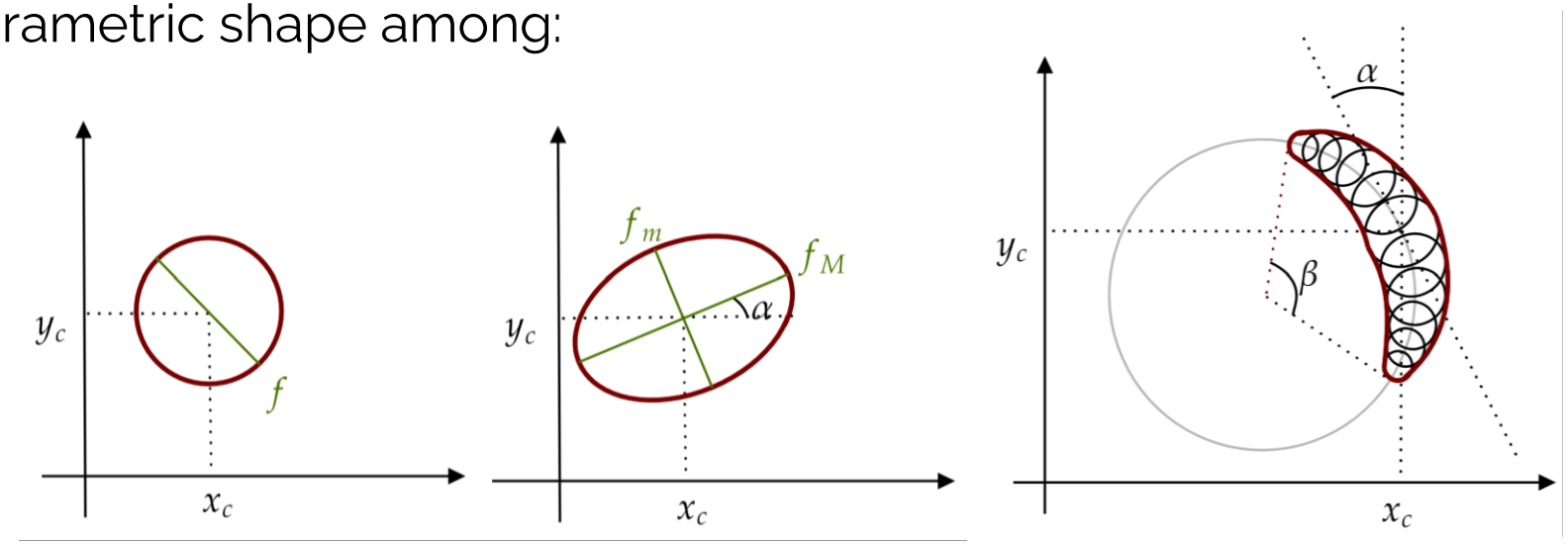

Figure: Gaussian shapes considered in the parametric imaging process.

and solve:

$$\underset{\theta\in\Theta}{\operatorname{argmin}} \quad \frac{1}{N_v - N_\theta} \sum_{k=1}^{N_v} \frac{|V_k - (\mathcal{F}\phi_\theta)_k|^2}{\sigma_k^2} \qquad (3)$$

Results – August 26, 2021

- Active region: AR2680
- 23:19:00 UT: GOES C4.0

STIX 6 – 10 keV
STIX 15 – 25 keV
AIA 1600 Å rotated

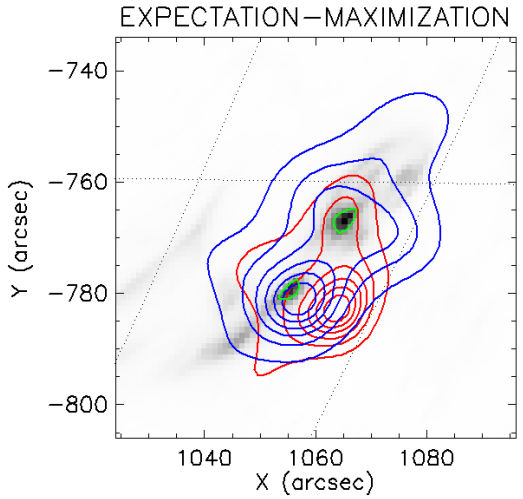

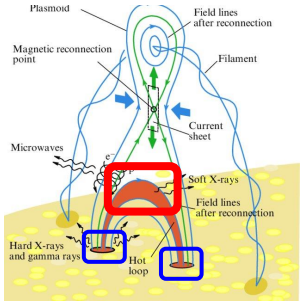

Figure: reconstructions provided by EM overlaid on the rotated AIA maps of the same events. Contour levels of the reconstructed thermal and non-thermal X-ray emissions are plotted in red and blue, respectively.

EXPECTATION MAXIMIZATION (Massa et al., Astronomy and Astrophysics, 2019)

- Count-based method
- Solves:

$$M\phi = C \tag{4}$$

EXPECTATION MAXIMIZATION (Massa et al., Astronomy and Astrophysics, 2019)

- Count-based method
- Solves:

$$M\phi = C \qquad (4)$$

Matrix modelling the grid transmission

EXPECTATION MAXIMIZATION (Massa et al., Astronomy and Astrophysics, 2019)

- Count-based method
- Solves:

$$M\phi = C \qquad (4)$$

Array containing the measured counts

Results – August 26, 2021

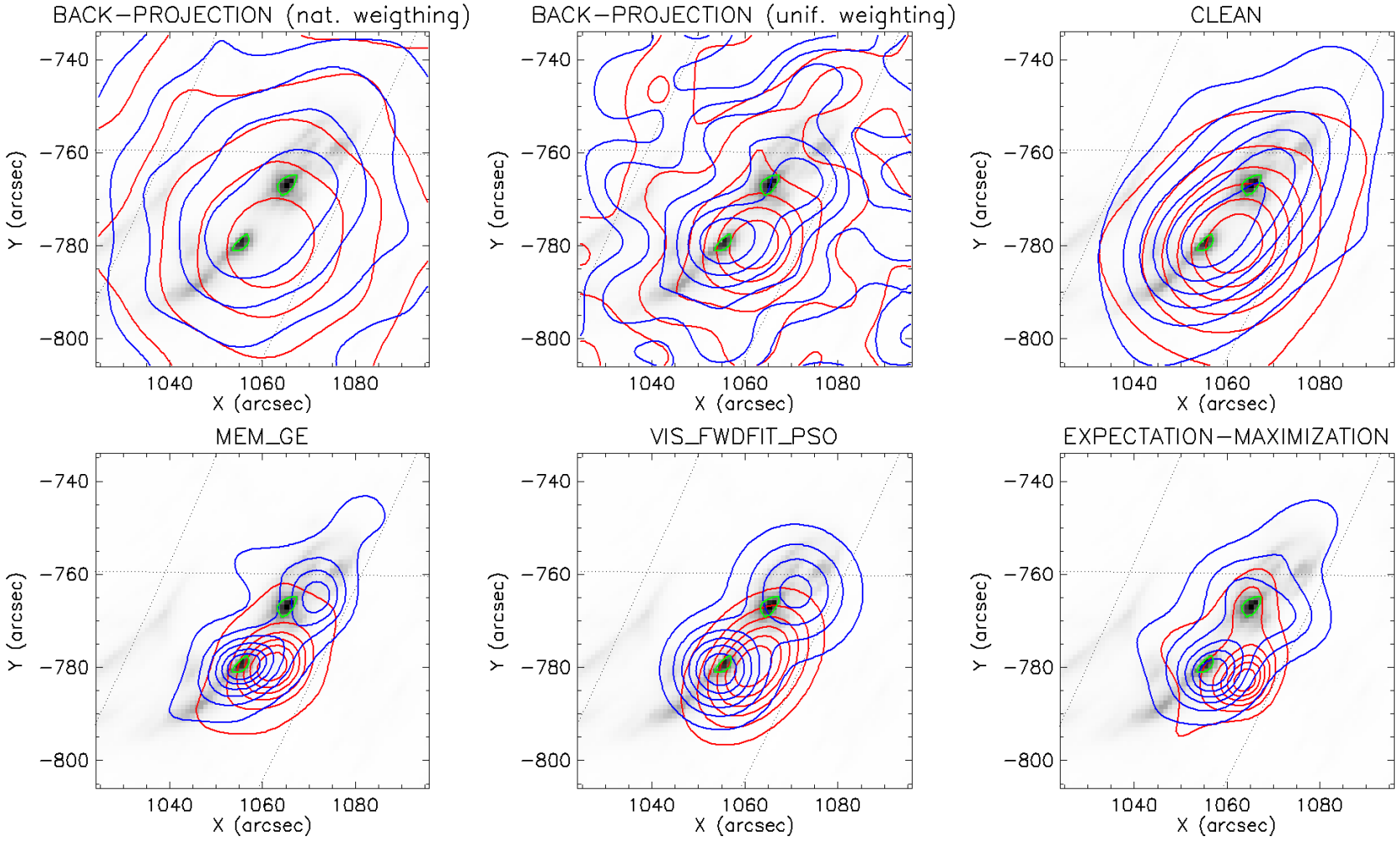

- Active region: AR2680
- 23:19:00 UT: GOES C4.0

STIX 6 – 10 keV
STIX 15 – 25 keV
AIA 1600 Å rotated

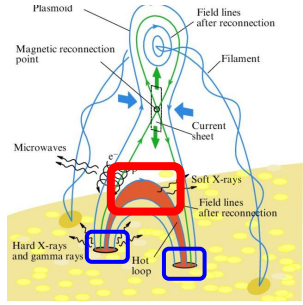

Figure: reconstructions provided by several methods overlaid on the rotated AIA maps of the same events. Contour levels of the reconstructed thermal and non-thermal X-ray emissions are plotted in red and blue, respectively.

Back-projection lines

- The back-projection of a single visibility is a sinusoidal wave defined by

$$\phi(x,y) = \mathcal{A}\cos(2\pi(xu+yv)-\omega)$$

where $\mathcal{A}$ and ω are the visibility amplitude and phase.

- We can associate to each visibility the set of lines corresponding to the maximum of the back-projection, i.e.,

$$2\pi(xu+yv)-\omega = 2\pi n, \qquad n \in \mathbb{Z}$$

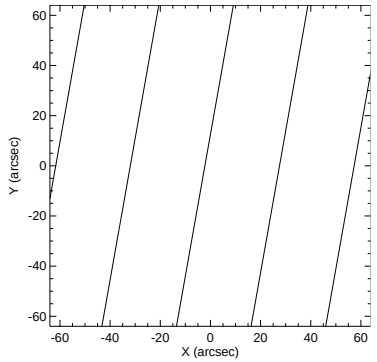

- If we assume that the observed X-ray source is a Gaussian circular source centered in (x_0, y_0), then one of the Back Projection lines passes through the center of the source.

$$\tilde{n} = \frac{2\pi(x_0 u + y_0 v) - \omega}{2\,\pi}$$

Back-projection Lines

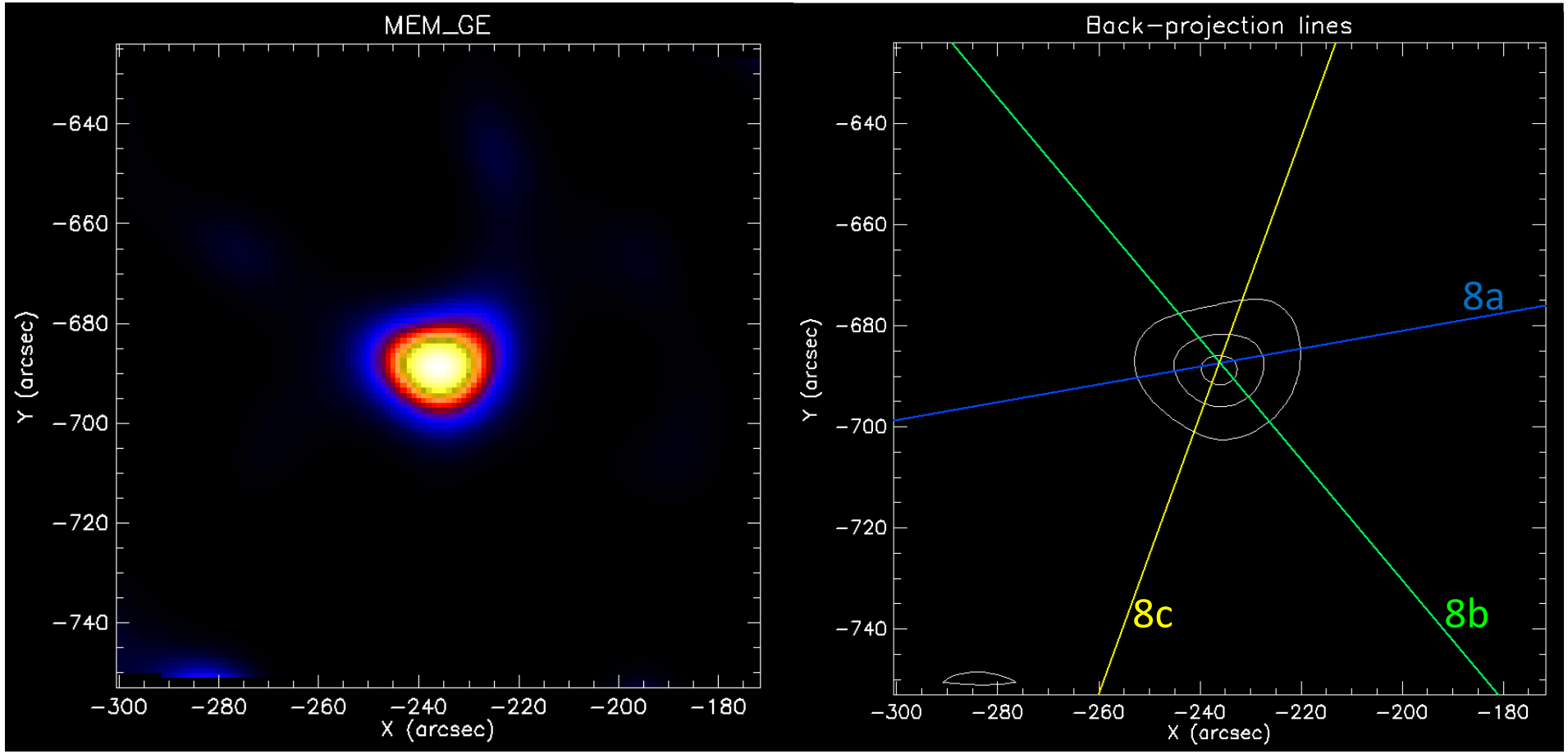

Figure: May 1, 2022 event recorded in the time interval 06:13:15 – 06:13:55 UT and in the energy range 6 – 9 keV. Left panel: reconstruction provided by MEM_GE. Right Panel: Back Projection lines of the three detectors with the same resolution overlaid to the MEM GE reconstruction.

Conclusions

- We described the STIX instrument and the image reconstruction problem from STIX data.
- We showed several imaging methods.
- We are working on the calibration of finest grids to get more detailed images.
- We are working on the implementation of new methods:
    - uv_smooth
    - MultiScale Clean

References

- Battaglia et al., *STIX X-ray microflare observations during the Solar Orbiter commissioning phase*, Astronomy and Astrophysics, (2021)
- Högbom, *Aperture synthesis with a non-regular distribution of interferometer baselines*, Astronomy and Astrophysics Supplement, (1974)
- Krucker et al., *The Spectrometer/Telescope for Imaging X-rays (STIX),* Astronomy and Astrophysics, (2020)
- Massa et al., *Count-based imaging model for the Spectrometer/Telescope for Imaging X-rays (STIX) in Solar Orbiter*, Astronomy and Astrophysics, (2019)
- Massa et al., *MEM_GE: A New Maximum Entropy Method for Image Reconstruction from Solar X-Ray Visibilities*, The Astrophysical Journal, (2020)
- Massa et al., *First hard X-ray imaging results by Solar Orbiter STIX*, Solar Physics, (2022)
- Meuris et al., *Caliste-SO, a CdTe based spectrometer for bright solar event observations in hard X-rays*, Nucl. Instrum. Methods Phys. Res. A, (2015)
- Perracchione et al., *Visibility interpolation in Solar Hard X-ray imaging: application to RHESSI and STIX*, The Astrophysical Journal, (2021).
- Piana et al., *Hard X-ray Imaging of Solar Flares*, Springer-Verlag, (2022)
- Volpara et al., *Forward-fitting STIX visibilities,* Astronomy and Astrophysics, (2022)

THANK YOU FOR THE ATTENTION!

Università di Genova
DIMA | Dipartimento di Matematica
MIDA group

n|w

Università di Genova